machines

MDPI

Article

A Novel Dynamic Modeling Framework for Flexure Mechanism-Based Piezoelectric Stick–Slip Actuators with Integrated Design Parameter Analysis

Xuan-Ha Nguyen and Duc-Toan Nguyen *

School of Mechanical Engineering, Hanoi University of Science and Technology, No. 1 Dai Co Viet Street, Bach Mai Ward, Hanoi 100000, Vietnam; ha.nguyenxuan@hust.edu.vn

* Correspondence: toan.nguyenduc@hust.edu.vn; Tel.: +84-988-693-047

Abstract

This paper presents an enhanced pseudo-rigid body model (PRBM) integrated with the LuGre friction law to analyze the dynamic behavior of flexure-hinge-based piezoelectric stick–slip actuators (PSSAs). The PRBM captures flexure compliance through Lagrangian dynamics, while Newtonian mechanics describe the piezoelectric stack and slider motion. Non-linear contact effects, including stick–slip transitions, are modeled using the LuGre formulation. A mass–spring–damper model (MSDM) is also implemented as a baseline for comparison. The models are solved in MATLAB Simulink version R2021a and validated against experimental data from a published prototype. The enhanced PRBM achieves strong agreement with experiments, with a root mean square error of 20.19%, compared to 51.65% for the MSDM. By reformulating the equations into closed-form expressions, it removes symbolic evaluations required in the standard PRBM, resulting in one to two orders of magnitude faster simulation time while preserving accuracy. Stable transient simulations are achieved at fine time steps ($\Delta t = 10^{-8}$ s). A systematic parametric study highlights preload force, flexure stiffness, friction coefficients, and tangential stiffness as dominant factors in extending the linear frequency–velocity regime. Overall, the PRBM–LuGre framework bridges the gap between computationally intensive finite element analysis and oversimplified lumped models, providing an accurate and efficient tool for design-oriented optimization of compliant piezoelectric actuators.

Keywords: piezoelectric stick–slip actuator; flexure hinge mechanism; dynamic modeling; pseudo-rigid body model; LuGre friction model; compliant mechanisms; system dynamics; micro-positioning

check for updates

Academic Editor: Hermes Giberti

Received: 25 July 2025
Revised: 26 August 2025
Accepted: 29 August 2025
Published: 1 September 2025

Citation: Nguyen, X.-H.; Nguyen, D.-T. A Novel Dynamic Modeling Framework for Flexure Mechanism-Based Piezoelectric Stick–Slip Actuators with Integrated Design Parameter Analysis. *Machines* **2025**, *13*, 787. https://doi.org/10.3390/machines13090787

Copyright: © 2025 by the authors. Licensee MDPI, Basel, Switzerland. This article is an open access article distributed under the terms and conditions of the Creative Commons Attribution (CC BY) license (https://creativecommons.org/licenses/by/4.0/).

1. Introduction

The rapid advancement of microsystem technologies has created an urgent demand for high-precision actuation systems capable of delivering ultra-fine resolution, compactness, and reliability in constrained environments. Among the diverse classes of precision actuators, piezoelectric stick–slip actuators (PSSAs) have emerged as particularly promising due to their ability to achieve nanometer-scale positioning, low power consumption, and superior miniaturization capabilities. These characteristics make PSSAs highly suitable for a wide range of applications, including micro-manipulation, biomedical devices, optical alignment systems, and micro-assembly platforms [1,2]. Since the pioneering work of Pohl in 1986 [3], PSSAs have undergone substantial design and performance improvements.

Numerous prototypes have been developed that integrate various structural and functional enhancements [4–9]. Currently, significant theoretical research has focused on aspects such as actuator miniaturization, control strategies, modeling accuracy, and optimization of performance metrics [6–9]. Despite these advances, there is a persistent research gap in the dynamic modeling of PSSAs, particularly those that incorporate flexure hinge mechanisms, a design feature increasingly adopted for its ability to enhance displacement amplification and adjust contact forces adaptively during actuation cycles.

In recent years, a substantial body of literature has explored the integration of flexure-based mechanisms into PSSA designs to improve their performance [10–19]. Flexure hinges offer dual functional advantages: they amplify the output displacement of piezoelectric stacks, thereby increasing the actuator stepping speed, and they provide compliant control over the normal contact force between the actuator and the slider. This not only enhances step length but also minimizes undesired backward motion (back-slip), reduces friction during the slip phase, and increases the actuator's load-carrying capacity. In doing so, they extend the operational lifespan by mitigating wear at the contact interface.

However, the use of flexure hinge mechanisms introduces additional complexities. Their inherently low stiffness can lead to low-frequency resonances, posing challenges in achieving stable high-speed control. The dynamic response of such systems is highly dependent on the geometric and mechanical properties of the flexure design. Therefore, the development of a comprehensive dynamic model that accurately captures these interactions is essential for performance prediction, controller design, and further optimization.

Most recent studies on flexure-based PSSAs [8–19] have concentrated on introducing new geometric designs, typically evaluated through finite element analysis (FEA) of quasi-static performance and then verified experimentally. While these works have significantly advanced actuator structures, they often overlook the strongly coupled dynamics among the piezoelectric stack, flexure hinges, frictional interfaces, and the slider, which ultimately govern transient stick–slip behavior.

Li et al. [10] demonstrated that FEA can effectively capture hinge deformation and locomotion accuracy in a two-stage flexure structure. Ding et al. [11] emphasized the importance of time-domain analysis for achieving smoother transient motion. Huang et al. [12] and Wang et al. [13,14] used FEA to assess structural symmetry, hinge geometry, and bio-inspired configurations, while Yang et al. [15] introduced perforated hinges and quantified compliance through FEA simulations. Optimization-driven approaches were also reported, with Ye [16] adopting distributed compliance and Zhang et al. [17] applying parallelogram mechanisms, both validated via FEA-based parametric studies. Sun et al. [18] and Yuan et al. [19] highlighted the role of FEA in evaluating compact and hybrid-drive actuators.

Although these contributions underscore FEA's effectiveness in structural design and validation, most analyses are limited to quasi-static or harmonic conditions, focusing on deformation, stress distribution, or modal behavior. Only a few studies attempt to perform transient simulations capable of capturing non-linear frictional interactions, stick–slip transitions, or chaotic dynamics at higher frequencies. This gap underscores the need for efficient dynamic models that balance physical accuracy and computational feasibility. To address this challenge, a unified modeling framework is needed that integrates the theory of compliant mechanisms with non-linear friction dynamics, providing a scalable and accurate approach for the transient analysis of flexure-based PSSAs.

Dynamic modeling efforts in the literature can generally be divided into two main approaches. The first relies on finite element analysis (FEA) [10–19], which is effective for capturing local stresses, modal behavior, and quasi-static deformation of flexure-based mechanisms. However, FEA-based transient analyses that resolve non-linear friction and

stick–slip transitions are rarely reported, mainly due to the high computational cost associated with wide frequency sweeps. The second approach employs lumped-parameter formulations, where the flexure hinge system is simplified as a mass–spring–damper (MSDM) model [20–25]. These models are computationally efficient and convenient for system-level simulation and control-oriented studies, yet they cannot represent the distributed compliance and non-linear stiffness intrinsic to flexure mechanisms. To address these limitations, this work introduces a structurally consistent pseudo-rigid body model (PRBM) [26], integrated with Lagrangian formulation and a friction model, to capture the coupled electromechanical and frictional dynamics of flexure-based PSSAs in the transient regime. Table 1 summarizes the two main dynamic modeling approaches for flexure-hinge-based PSSAs, and highlights how the proposed PRBM–LuGre framework differs in terms of friction modeling, flexure representation, and system-level dynamic coupling.

Table 1. Comparison of modeling methods for flexure-hinge-based stick–slip actuators.

Approach	Friction Model	Flexure Mechanism Model	Dynamic Coupling
FEA-based	None explicitly	Flexure mechanism evaluated with static/ harmonic FEA [10–19]	Quasi-static or modal only
Lumped MSDM	LuGre or single-state friction [27–29]	Flexures approximated by mass–spring–damper elements [20–25]	Yes, but oversimplified
This work (PRBM–LuGre)	LuGre	Flexures modeled with PRBM and Lagrangian formulation	Full electromechanical–frictional coupling with parametric analysis

Several friction modeling approaches have been applied in the context of PSSAs. The classical Coulomb model is simple to simulate but cannot capture key effects such as presliding displacement, Stribeck behavior, and viscous friction [30,31]. Contact mechanics combined with the dimensionality reduction method [31–34] provides a more detailed description of friction phenomena with reduced computational cost, though it is restricted to specific cases such as sphere–plane contacts. Single-state dynamic models, such as the Dahl-based formulation [27–29], are more widely used since they can be applied to arbitrary contacts and allow rapid dynamic simulations. For actuators operating at the micrometer scale, these models have proven sufficient in many studies [20–22,35–38]. Given these requirements and prior findings, adopting a dynamic bristle formulation like the LuGre model [28] is particularly suitable for flexure-based PSSAs, as it combines presliding hysteresis with Stribeck and viscous effects while remaining computationally tractable.

This study seeks to bridge the aforementioned gap by proposing a novel and unified dynamic modeling framework for flexure-based PSSAs. Unlike previous works that rely on lumped parameter models, our approach integrates a multi-domain representation encompassing rigid-body dynamics, flexural deformation, and non-linear friction behavior. Specifically, the dynamics of the slider and piezoelectric actuator are formulated using Newtonian mechanics. The flexure hinge mechanism is modeled using the PRBM in conjunction with the second-kind Lagrange equations, enabling an accurate capture of elastic deformation while preserving computational tractability. The frictional interaction between the slider and the guide surface is described using the LuGre dynamic friction model [28], which allows for capture of both spring-like characteristics and velocity-dependent hysteresis effects.

To demonstrate the generalizability and effectiveness of the proposed methodology, we select a previously published flexure-based PSSA prototype introduced by Sun et al. [18] as a representative case study. The integrated dynamic model is implemented and numerically simulated in MATLAB Simulink version 2021a, and its predictions are validated against experimental results reported in [18]. Sensitivity analyses are performed to quantify the influence of critical design parameters, including the preload force, friction coefficient, tangential contact stiffness, flexure joint stiffness, center-of-mass positioning, and slider mass, on the actuator's frequency–velocity performance.

The key contributions of this work are as follows:

- We develop a comprehensive dynamic model of a flexure-based PSSA that rigorously captures the coupled dynamics of its constituent subsystems.
- We introduce a hybrid modeling approach that combines PRBM, Newtonian dynamics, Lagrangian mechanics, and the LuGre friction model in a unified framework.
- We provide a quantitative analysis of the effects of design parameters on dynamic behavior, offering valuable guidelines for actuator optimization.
- We establish a generalized modeling strategy that can be readily extended to a wide variety of PSSA designs that employ flexure hinge mechanisms.

To further highlight the advantages of the proposed modeling approach, a simplified mass–spring–damper model (MSDM) is also developed and evaluated in parallel. This benchmark model, commonly adopted in prior studies, treats the flexure-based actuator as a lumped second-order system with equivalent stiffness and damping. By comparing simulation outcomes from both models under identical input conditions, we systematically assess modeling accuracy, computational efficiency, and sensitivity to design parameters.

This research provides a foundational step toward predictive modeling, design automation, and intelligent control of next-generation PSSAs. By highlighting the dynamic interdependencies within these systems, our work enables both researchers and engineers to achieve enhanced performance and reliability in micro-positioning applications.

2. System Modeling and Benchmark MSD Model

To facilitate clarity in presenting the novel contributions of this research, a concise overview of the mechanical structure and operating principle of the actuator, originally introduced by Sun et al. [18] is provided herein. Although comprehensive design details are fully documented in the referenced study, we reiterate the essential aspects that underpin the dynamic modeling framework developed in this work.

As illustrated in Figure 1a, the actuator consists of five main parts, including the piezo-stack element, the four-bar mechanism based on the flexure hinge structure, the slider mounted on a linear ball bearing, the frictional driving contact between the slider and the four-bar mechanism, and the preload adjustment screw. The preload screw is used to adjust the preload applied to the frictional contact. All components are installed integrally on a mechanically rigid base platform to ensure consistent motion transmission and structural integrity. The actuation principle is based on the stick–slip mechanism, which enables precision micro-positioning. As shown in Figures 1b,c, a sawtooth voltage signal excites the piezo-stack element, causing it to extend slowly in the forward stroke and retract rapidly in the return stroke. This asymmetry in actuation velocity facilitates the incremental displacement of the slider via frictional coupling. Due to the inherently limited stroke length of the piezo-stack (typically of the order of a few micrometers), the flexure-based four-bar mechanism serves as a mechanical amplifier, significantly increasing the output stroke transmitted to the slider. The magnitude of the frictional force—crucial for ensuring stick–slip motion—is modulated through the preload screw, which alters the normal force at the contact interface.

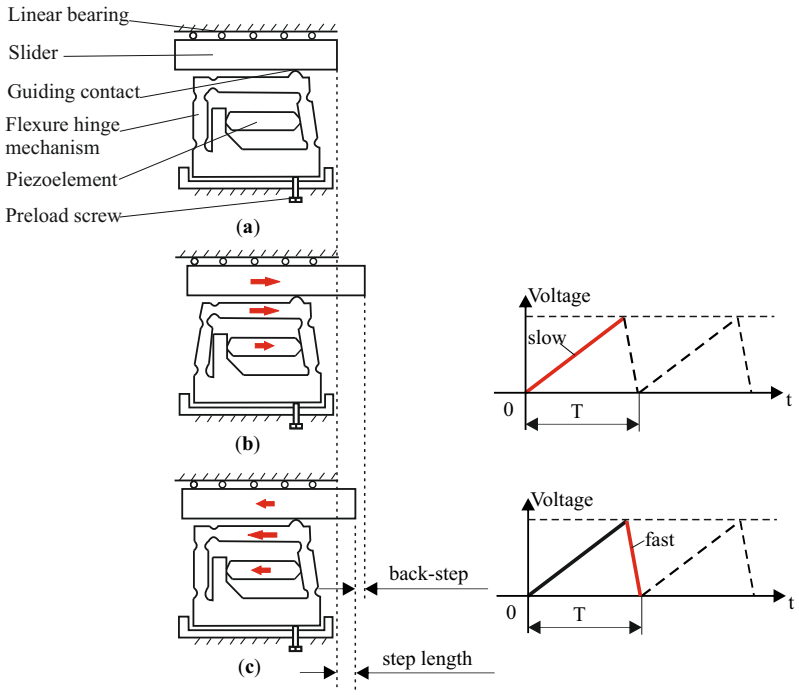


Figure 1. Structural design and operational principle of the stick–slip actuator [18]: (**a**) Initial configuration, (**b**) Stick phase under slow expansion of the piezoelectric stack, and (**c**) Slip phase during rapid contraction.

2.1. PRBM–LuGre Dynamic Modeling Framework

A key innovation of this study lies in the application of the pseudo-rigid body model (PRBM) [26] for an accurate dynamic characterization of the flexure-based four-bar mechanism. As depicted in Figure 2, the mechanism is modeled as a planar four-bar link consisting of four rigid links interconnected by compliant revolute joints. At each joint, a torsional spring is used to connect two rigid bars. The springs have an elastic modulus k_i, which represents the elasticity of the flexural joints. Each bar of the four-bar mechanism has a kinematic dimension l_i. The position of each bar is determined by φ_i. The center of gravity of each bar is determined by r_i and β_i. The mass m_i and the moment of inertia I_i represent the dynamic parameters of the bar. For all parameters, the subscription i is in a range from 1 to 4.

The piezo-actuator is modeled as a mass–spring–damper system with three parameters m_p, k_p, and c_p, which represent the mass, stiffness, and damping coefficient of the actuator, respectively. The connecting joint between the piezo-element and the flexure mechanism at point A is modeled as a linear spring with stiffness k_u. The left end of the piezo-element is considered to be rigid and fixed to the flexure mechanism. The position of point A is defined by x_a, determined from l_a. The saw-tooth driving voltage applied to the piezo-element is expressed by x_p. The displacement of the piezo-element and the contact point C is defined by x_u and x_c, respectively. Since the displacement resolution of the considered drive is in the micrometer range, other non-linear characteristics of the piezoelement, including hysteresis and aging, are neglected. These non-linear characteristics are significant only in the nanometer range.

A detailed free-body diagram of the interaction between the slider and the flexure mechanism is illustrated in Figure 2, which emphasizes the key dynamic interactions that occur at the contact interface. At the contact point C, there appears a friction force F_f and a normal force F_N. The slider is mounted on a linear ball bearing, which constrains its motion to a single translational degree of freedom along the x-axis. It has an effective mass m_s, and its displacement is denoted by x_s. The slider receives motion exclusively

through the tangential component of the contact force generated at point *C*, where the flexure mechanism interfaces with the slider.

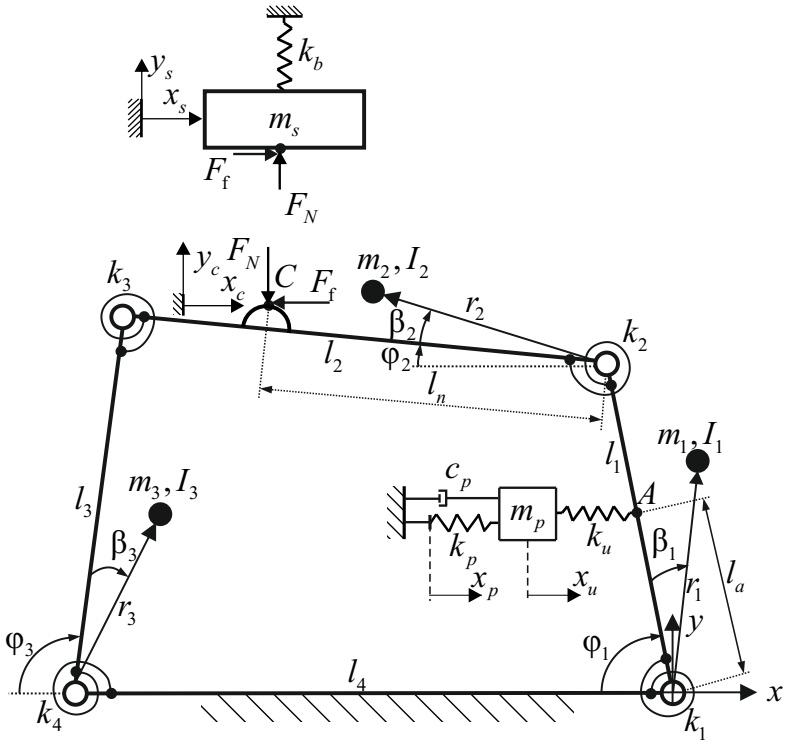


Figure 2. Free body diagram of dynamic system modeling.

The dynamic equation of the flexure mechanism is established using the Lagrange formulation as in Equation (1). Details of the deviation can be found in [39]. The full form of the dynamic equation is written in the following way.

$$\frac{d}{dt}\left(\frac{\partial K}{\partial \dot{\varphi}_1}\right) - \frac{\partial K}{\partial \varphi_1} + \frac{\partial P}{\partial \varphi_1} = \tau \tag{1}$$

where K, P, and τ denote the kinetic energy, the potential energy, and the external input torque, respectively. The motion of the four-bar mechanism is described by the input angle φ_1.

The kinetic energy of the mechanism can be calculated as

$$K = \sum_{i=1}^{3}\left[\frac{1}{2}m_i(V_{ix}^2 + V_{iy}^2) + \frac{1}{2}I_i\dot{\varphi}_i^2\right] \tag{2}$$

where $\dot{\varphi}_i$ and V_{ix}, V_{iy} represent the angular velocity and the x- and y-axis velocity components of the center mass of the bar i.

Equation (2) can be re-written in substitution form

$$K = \frac{1}{2}A(\varphi_1){\dot{\varphi}_1}^2 \tag{3}$$

where $A(\varphi_1)$ is determined by

$$A(\varphi_1) = \sum_{i=1}^{3}\left[m_i\frac{V_{ix}^2 + V_{iy}^2}{{\dot{\varphi}_1}^2} + I_i\frac{\dot{\varphi}_i^2}{{\dot{\varphi}_1}^2}\right] \tag{4}$$

$$A(\varphi_1) = C_0 + C_1\omega_2^2 + C_2\omega_3^2 + C_3\omega_2 cos(\varphi_2 - \varphi_1 + \beta_2) \tag{5}$$

in which ω_2 and ω_3 are the angular velocity of bar 2 and 3 depending on the angular velocity of bar 1. The calculation of these parameters can be found in Appendix I of [39]. The coefficient C_i ($i = 0 - 3$), depending on the parameters of the mass distribution, is given as

$$C_0 = I_1 + m_1 r_1^2 + m_2 l_1^2;\ C_1 = I_2 + m_2 r_2^2;\ C_2 = I_3 + m_3 r_3^2;\ C_3 = 2 m_2 r_2 l_1. \tag{6}$$

The potential energy of the mechanism is calculated as

$$P = P_s + P_g \tag{7}$$

where P_s and P_g are the potential energy stored in the torsional springs and the potential energy created by gravity. Calculation of these parameters is given by

$$\begin{aligned} P_s = \frac{1}{2}[&k_1(\varphi_1 - \varphi_1^0)^2 + k_2(\varphi_2 - \varphi_1 + \varphi_1^0 - \varphi_2^0)^2 \\ &+ k_3(\varphi_3 - \varphi_2 + \varphi_2^0 - \varphi_3^0)^2 + k_4(\varphi_3 - \varphi_3^0)^2], \end{aligned} \tag{8}$$

and

$$\begin{aligned} P_g = g[&m_1 r_1 sin(\varphi_1 + \beta_1) + m_2(l_1 sin\varphi_1 + r_2 sin(\varphi_2 + \beta_2)) + \\ &+ m_3(l_4 sin\varphi_4 + r_3 sin(\varphi_3 + \beta_3))], \end{aligned} \tag{9}$$

where φ_i^0 ($i = 1 - 3$) is the initial position of the bar i corresponding to zero deflection of the torsional springs; g is the gravity coefficient; k_i ($i = 1 - 4$) depend on the geometric parameters of flexible joints, including the elastic modulus E, thickness e, radius r, and width b [40]:

$$k_i = \frac{2Ebe^{\frac{5}{2}}}{9\pi\sqrt{r}}. \tag{10}$$

Calculating the derivative components of the potential energy and the kinetic energy, we obtain Equations (11)–(14). Substituting these equations into Equation (1), we have Equation (15).

$$\begin{aligned} \frac{\partial P_s}{\partial \varphi_1} = &k_1(\varphi_1 - \varphi_1^0) + k_2(\varphi_2 - \varphi_1 + \varphi_1^0 - \varphi_2^0)(\omega_2 - 1) + \\ &+ k_3(\varphi_3 - \varphi_2 + \varphi_2^0 - \varphi_3^0)(\omega_3 - \omega_2) + k_4(\varphi_3 - \varphi_3^0)\omega_3 \end{aligned} \tag{11}$$

$$\begin{aligned} \frac{\partial P_g}{\partial \varphi_1} = &g[m_1 r_1 cos(\varphi_1 + \beta_1) + m_2(l_1 cos\varphi_1 + r_2 cos(\varphi_2 + \beta_2)\omega_2) + \\ &+ m_3 r_3 cos(\varphi_3 + \beta_3)\omega_3] \end{aligned} \tag{12}$$

$$\frac{d}{dt}\left(\frac{\partial K}{\partial \dot{\varphi_1}}\right) = A(\varphi_1)\ddot{\varphi}_1 + \frac{\partial A(\varphi_1)}{\partial \varphi_1}\dot{\varphi_1}^2 \tag{13}$$

$$\frac{\partial K}{\partial \varphi_1} = \frac{1}{2}\frac{\partial A(\varphi_1)}{\partial \varphi_1}\dot{\varphi_1}^2 \tag{14}$$

$$A(\varphi_1)\ddot{\varphi}_1 + \frac{1}{2}\frac{\partial A(\varphi_1)}{\partial \varphi_1}\dot{\varphi_1}^2 + \frac{\partial P_s}{\partial \varphi_1} + \frac{\partial P_g}{\partial \varphi_1} = \tau \tag{15}$$

The external input torque τ in Equation (15) depends on the interaction between the flexure mechanism with the piezo-element and the slider. This torque will be calculated in the next section.

The dynamic equation of the piezo-actuator is based on Newtonian mechanics as follows:

$$m_p \ddot{x_u} = k_u(x_a - x_u) - c_p(\dot{x_u} - \dot{x_p}) - k_p(x_u - x_p), \tag{16}$$

where x_a is calculated from the position of bar 1 as

$$x_a = l_a(cos\varphi_1^0 - cos\varphi_1) \tag{17}$$

The dynamic motion of the slider in the x-direction is described as:

$$m_s \ddot{x_s} = F_f \tag{18}$$

where F_f is the friction force between the slider and the flexure mechanism at the contact point A, which needs to be modeled.

The friction force depends on the normal force and the contact property. The friction force is modeled using the single-state friction model called the LuGre model [28]. The normal force depends on the preload applied to the flexure mechanism and the dynamic behavior of the flexure mechanism. The friction force is modeled as:

$$F_f = \sigma_0 z + \sigma_1 \frac{dz}{dt} + \sigma_2 v, \tag{19}$$

where σ_0, σ_1, and σ_2 are the equivalent-tangential stiffness, damper, and viscous friction coefficient; v is the relative velocity between the slider v_s and the flexure mechanism v_c at the contact point C.

$$v = v_c - v_s, \tag{20}$$

The model contains a continuous state variable z representing the average deflection of the asperity conjunctions of the contact. This parameter is defined as follows:

$$\frac{dz}{dt} = v - \frac{|v|}{g(v)} z \tag{21}$$

where $g(v)$ captures the Coulomb friction and the Stribeck effect.

$$g(v) = \frac{F_C + (F_S - F_C)e^{-(v/v_S)^2}}{\sigma_0}, \tag{22}$$

where F_S corresponds to the stiction force, F_C is the Coulomb friction force, and v_s is the Stribeck velocity. F_S and F_S are called normal forces F_N and the corresponding friction coefficients are μ_S and μ_C:

$$\begin{cases} F_S = F_N \mu_S \\ F_C = F_N \mu_C \end{cases}. \tag{23}$$

To complete the dynamic modeling of the actuation system, we derive the torque balance equation for the flexure mechanism under the influence of contact forces. The total external torque acting on the mechanism is expressed as:

$$\tau = l_a sin\varphi_1 k_u(x_u - x_a) - F_N(l_1 cos\varphi_1 + l_n cos\varphi_2) - F_f(l_1 sin\varphi_1 + l_n sin\varphi_2). \tag{24}$$

This section presents a novel and comprehensive contact force modeling framework that integrates mechanical amplification and friction-based actuation through a PRBM

augmented with the dynamic LuGre friction model. In contrast to conventional static or overly simplified approaches, the proposed model accurately captures non-linear geometric deformations in flexure mechanisms, the coupled dynamics between the compliant transmission and the piezoelectric actuator, and the influence of adjustable preload on stick–slip transitions. By realistically modeling tribological interactions and dynamic responses, this framework enables high-fidelity simulations and control-oriented designs of compact high-resolution actuators. Its scientific significance lies in bridging the gap between theoretical modeling and practical implementation, providing a robust foundation for optimizing next-generation piezo-driven compliant mechanisms in applications such as micro-positioning, scanning systems, and adaptive optics.

2.2. Mass–Spring–Damper (MSD) Model

To benchmark the advantages of the proposed modeling approach, a dynamic model based on a conventional method from previous studies [20–25] is also developed for comparison. In this traditional modeling approach, referred to as the mass–spring–damper (MSD) method, the flexure hinge mechanism is highly simplified and represented as a lumped-parameter system composed of masses, springs, and dampers. The dynamic parameters of the system are empirically identified, often based on experimental fitting or engineering experience. As a result, structural design parameters related to geometry and material properties are qualitatively captured and cannot be explicitly incorporated into the dynamic model. Consequently, the influence of each design parameter on the global system dynamics cannot be directly assessed using this method.

Following the MSD approach, the prototype developed by Sun et al. is modeled as a system of interconnected mass–spring–damper components. As illustrated in Figure 3, the piezoelectric actuator is modeled using parameters m_p, k_p, and c_p, representing its effective mass, stiffness, and damping coefficient, respectively. Similarly, the four-bar flexure hinge mechanism is modeled with equivalent mass m_e, stiffness k_e, and damping c_e. The input to the actuator is a sawtooth voltage signal, represented by x_p. The displacement of the actuator and the contact point C are denoted by x_u and x_c, respectively, while the slider displacement is expressed as x_s. The slider, with mass m_s, moves under the influence of the friction force F_f, which is evaluated based on the set of Equations (19)–(23). The equations of motion for the piezoelectric actuator and the flexure hinge mechanism are derived using Newtonian mechanics and presented in Equations (25) and (26), respectively.

$$m_p\ddot{x_u} = k_p(x_p - x_u) + k_e(x_c - x_u) + c_p(\dot{x_p} - \dot{x_u}) + c_e(\dot{x_c} - \dot{x_u}) \tag{25}$$

$$m_e\ddot{x_c} = k_e(x_u - x_c) + c_e(\dot{x_u} - \dot{x_c}) - F_f \tag{26}$$

While the MSD model offers computational simplicity and serves as a convenient baseline, it has clear limitations. In particular, the lumped-parameter representation does not reflect the distributed compliance or non-linear stiffness of the flexure hinges, and the dynamic parameters are typically tuned empirically rather than derived from the structural and material properties. As a result, the MSD framework cannot capture the influence of specific design variables, such as hinge geometry or preload stiffness, on the overall actuator dynamics. In contrast, the proposed PRBM–LuGre model preserves structural fidelity by incorporating compliant joint mechanics and non-linear friction dynamics, enabling accurate prediction of transient behavior as well as systematic parametric studies. This distinction underscores the advantage of the PRBM-based framework as a more physically consistent and predictive tool for analyzing flexure-based PSSAs.

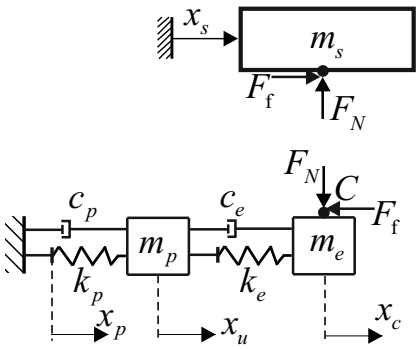


Figure 3. Schematic illustration of the dynamic system using the MSD (mass–spring–damper) approach, where the piezoelectric actuator and the flexure hinge mechanism are represented by lumped parameter elements. This simplified model serves as a baseline for comparison with the proposed PRBM-based modeling framework.

3. Numerical Simulation and Validation

To simulate and validate these complex dynamics, a comprehensive numerical model was developed in MATLAB Simulink, as illustrated in Figure 4. The Simulink model consists of four main subsystems: piezoelectric input, flexure compliance, LuGre friction, and load mass. The outputs include the displacements of the piezo stack (x_p), flexure point (x_a), and slider (x_s), together with velocity signals from which frequency–velocity responses are computed. Full simulation details are available upon request. Parameter values were carefully selected and, where applicable, derived from empirical data reported in [18], ensuring realistic modeling fidelity. These are summarized in Tables 1–4, and the simulation parameters are calculated and chosen as in Table 2 for the LuGre friction model, Table 3 for the piezo-element and the slider, and Table 4 for the four-bar mechanism.

Table 2. Parameters of LuGre friction model used in simulations.

Parameters	Notation	Value
Tangential stiffness	σ_0	2×10^6 (5×10^6, 1×10^7) (N/m)
Damper coefficient	σ_1	5 (Ns/m)
Viscous friction coefficient	σ_2	0.5 (Ns/m)
Static friction coefficient	μ_S	0.15 (0.25, 0.3)
Coulomb friction coefficient	μ_C	0.1 (0.15, 0.2)
Stribeck velocity	v_s	0.001 (m/s)

Note: Friction parameters are obtained from experimental data in [18]. The static and dynamic coefficients are directly extracted from the measured normal force–friction dependency curves, while the empirical parameters σ_0, σ_1, and σ_2 are estimated from the contact geometry and material properties in [18], following the approach of [35].

Table 3. Parameters of the piezo-element and the slider.

Parameters	Notation	Value
Stiffness coefficient	k_p	3.6×10^6 (N/m)
Damper coefficient	c_p	0.294 (Ns/m)
Mass of the piezo	m_p	15 (g)
Stiffness of connecting joint	k_u	3×10^6(3×10^7, 8×10^7) (N/m)
Mass of the slider	m_s	100 (50, 10) (g)
Distance defining position of point A	l_a	5.1 (mm)
Distance defining position of point C	l_n	0 (5, 10, 15) (mm)
Preload	F_p	20(15, 10, 5, 1) (N)

Note: Dynamic parameters of the piezoelectric element are calculated from its material properties and dimensions reported in [18], converted into equivalent lumped values using the reduced mass method [35]. The joint stiffness k_u is derived from flexure geometry and material properties, while the preload force F_p is taken directly from the experimental setup in [18].

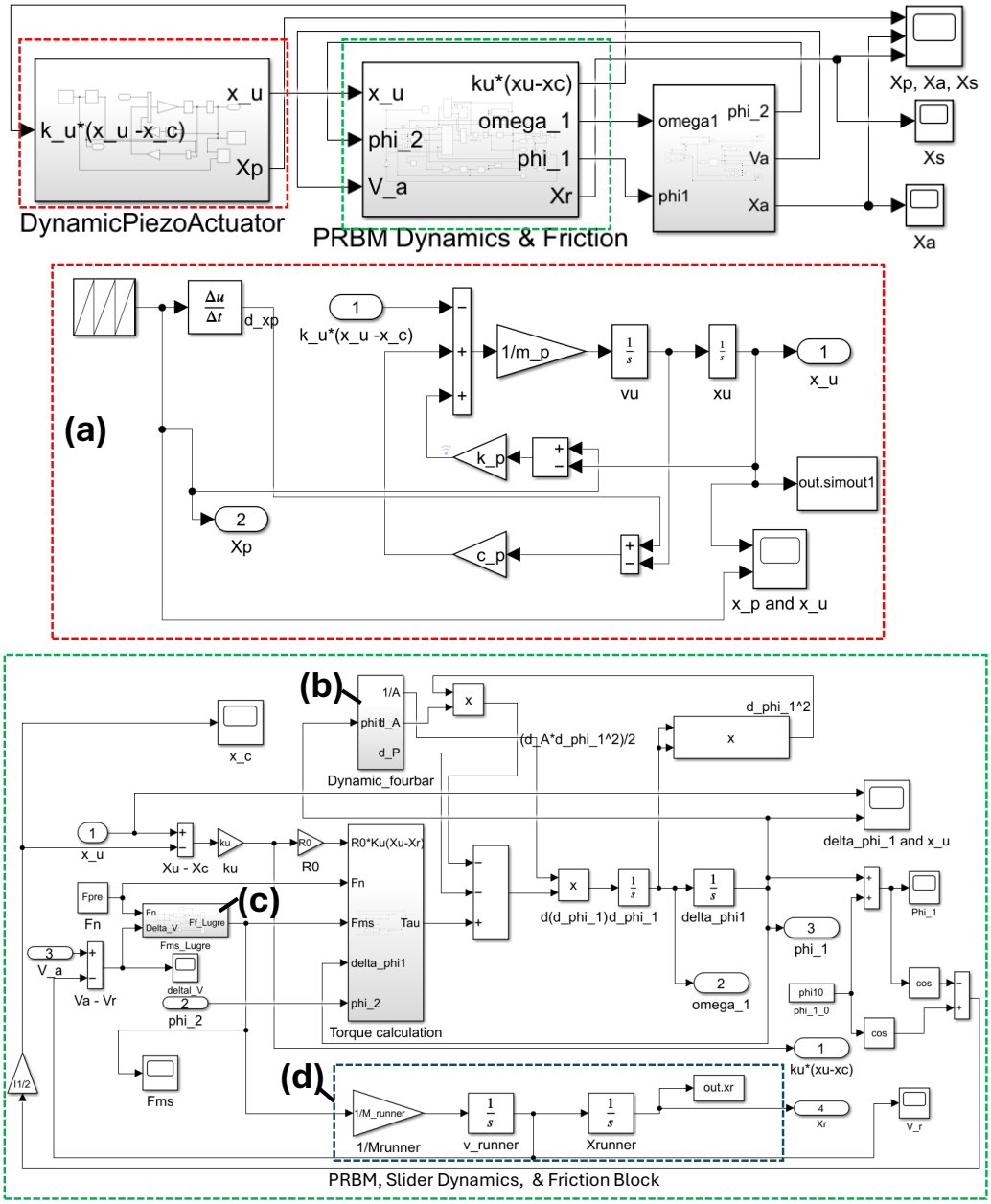


Figure 4. MATLAB/Simulink block diagram of the proposed dynamic model. The system consists of four main subsystems: (**a**) the piezoelectric input block, which generates the sawtooth displacement excitation; (**b**) the flexure compliance block, implementing the PRBM-based four-bar mechanism via the Lagrangian formulation; (**c**) the LuGre friction block, which models stick–slip transitions at the contact interface; and (**d**) the load mass block, representing the slider dynamics. The outputs include the piezo stack displacement (x_p), flexure point displacement (x_a), and slider displacement/velocity ($x_s, \dot{x}_s$), from which frequency–velocity response characteristics are computed.

A fundamental aspect of the dynamic behavior of piezoelectric stick–slip actuators (PSSAs) is the presence of micro-vibrations that emerge immediately after the slip phase. These high-frequency oscillations are primarily induced by the rapid reversal in the deformation of the piezoelectric element, which dynamically interacts with the flexure hinge mechanism of the system and the frictional characteristics at the guiding interface. The interplay of these factors, namely, the inertia and compliance of the flexure structure, the piezoelectric actuation, and the stick–slip contact friction, governs the system's transition into either stable or chaotic regimes.

Table 4. Parameters of the four-bar flexure hinge mechanism.

Parameters	Notation	Value
Elastic modulus	E	72 (GPa)
Mass density	D	2810 (kg/m^3)
Length of link 1	l_1	10.2 (mm)
Length of link 2	l_2	23.2 (mm)
Length of link 3	l_3	10 (mm)
Length of link 4	l_4	25 (mm)
Mass of link 1	m_1	0.2568 (g)
Mass of link 2	m_2	0.5877 (g)
Mass of link 3	m_3	0.2529 (g)
Width of link	b	3 (mm)
Height of link	h	3 (mm)
Thickness of joint	e	1.5 (mm)
Radius of joint	r	1 (mm)
Initial position of link 1	φ_1^0	80°
Initial position of link 2	φ_2^0	0°
Initial position of link 3	φ_3^0	270°
Initial position of link 4	φ_4^0	180°
Equivalent mass of the mechanism	m_e	0.589 (g)
Equivalent stiffness coefficient	k_e	2.88×10^6 (N/m)
Equivalent damping coefficient	c_e	218 (Ns/m)

Note: The geometric and material parameters of the flexure-based four-bar mechanism are identical to those in [18]. For the MSDM, the dynamic parameters of the compliant mechanism are obtained using the equivalent lumped-parameter method, ensuring consistency with the low-frequency behavior of the actual structure.

When the actuator is driven at low excitation frequencies, the micro-vibrations are efficiently suppressed during the subsequent stick phase because of the inherent damping and frictional resistance. This leads to a periodic linear motion, and the system operates predictably and stably. In contrast, at higher driving frequencies, the residual micro-vibrations are no longer fully attenuated before the next actuation cycle begins. This incomplete damping causes cumulative oscillations that eventually result in chaotic motion of the slider, severely affecting positioning precision and system stability [2,33,34,36].

To characterize and visualize this phenomenon, dynamic simulations were performed at two representative frequencies, 1.5 kHz and 1.405 kHz, as shown in Figure 5. At each frequency, both the displacement trajectories of the slider and the piezoelectric element, which depend on the time, are shown. In both cases of simulated frequency, residual micro-vibrations from the preceding cycle significantly influenced the starting condition of the subsequent cycle, thereby altering the net step length of the slider. The relative phase shift between the slider and the piezo-element was found to either augment or diminish the displacement per cycle, depending on their direction of motion. Specifically, Figure 5a illustrates a case where opposing motions lead to a reduction in step length, while Figure 5b shows a scenario in which aligned motions cause an increase.

$$v = f \cdot S \tag{27}$$

The average velocity of the slider, which depends on frequency and step length, is determined by Equation (27). Thus, if the step length is constant, the slider's average velocity increases linearly with increasing driving frequencies. However, at high driving frequencies, the residual micro-vibrations lead to variances in the step length. As a result, the slider's average velocity will be unstable if the micro-vibration is not fully suppressed within the following stick phase. Furthermore, when the driving frequency increases beyond a certain threshold, called the critical frequency, a slip between the slider and the

contact element can appear even in the current stick phase. This slip will lead to a large decrease in the step length, and consequently in the slider's average velocity. The critical frequency is determined based on two conditions, including no residual micro-vibrations at the end of the following stick phase and no slip within the current stick phase. It can be seen in Figures 6–14 below that, beyond the critical frequency, the slider velocity will be reduced.

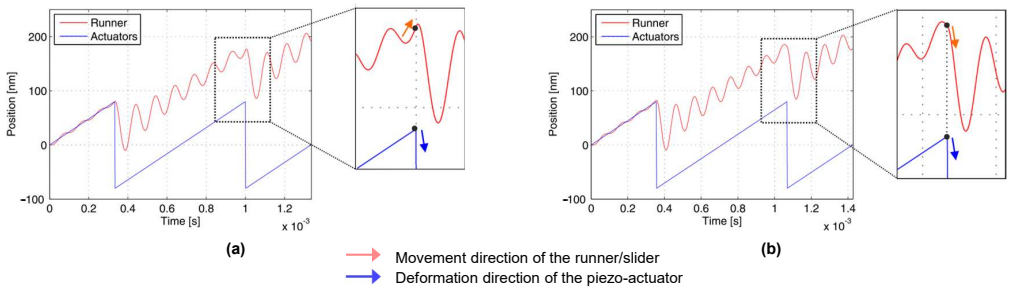


Figure 5. Illustration of chaotic behavior induced by micro-vibration: (**a**) Driving at a frequency of 1.5 kHz. (**b**) Driving at a frequency of 1.405 kHz.

For the analysis of the design parameters, several testing scenarios were performed. In the first scenario, a simulation with the same parameters as in [18] was performed and compared with the experimental data. In other scenarios, some important design parameters are changed to evaluate their influence on the dynamic behavior of the whole system, expressed by the frequency–velocity dependence. For each of the following scenarios, only one parameter is changed while the other parameters remain the same as in the first scenario. The values in parentheses are the changing parameters used in the simulations. The changed parameters include the following: preload F_p, center of gravity position of each bar β_i, contact position l_n, slider mass m_s, tangential stiffness σ_0, friction coefficient μ_S, μ_C, and stiffness of the flexure hinge k_u.

A series of simulation trials were performed to systematically assess the influence of these parameters on the dynamic performance of the system, with a specific focus on the velocity–frequency response as a diagnostic metric to identify transition thresholds between stable and chaotic operation. To validate the simulation results, the results were compared with the experimental data obtained from [18].

The measured and simulated slider velocities as functions of the driving frequency are presented in Figure 6. In the experimental setup, the driving frequency was varied from 100 Hz to 1500 Hz in increments of 100 Hz. For the simulations, the frequency range was extended from 100 Hz to 2000 Hz using the same step resolution. The simulation results obtained using both the proposed PRBM and the MSDM are plotted alongside the experimental data for comparison. While validation is performed up to 1.5 kHz, simulations are extended to 2 kHz to illustrate the extrapolation capability of the model for potential future actuator designs. It is emphasized that results beyond 1.5 kHz are predictive in nature and not experimentally validated.

The simulation results obtained using the PRBM are analyzed and compared with the experimental data, as shown in Figure 6. It is observed that, for frequencies below 900 Hz, the numerical simulation shows good agreement with the experimental results in terms of both trend and amplitude. In this frequency range, the frequency–velocity relationship exhibits predominantly linear behavior. This linearity can be explained by the fact that, at low driving frequencies, micro-vibrations are fully suppressed before the initiation of a new actuation cycle. As a result, the system remains stable without any chaotic behavior, and the step length of the slider remains constant. Consequently, the average velocity increases proportionally with frequency. In contrast, when the driving frequency exceeds

900 Hz, the time available in each cycle becomes too short to allow complete suppression of micro-vibrations. These residual micro-vibrations introduce instability into the system, which can lead to chaotic dynamics and cause the velocity response to become non-linear. Due to this non-linear nature, even a small change in the driving frequency can result in large, unpredictable variations in the slider's velocity. Therefore, in practical applications, the device is typically operated within a frequency range where the frequency–velocity relationship remains linear to ensure predictable and stable performance. Moreover, at high frequencies, slipping can occur even during the stick phase due to the influence of residual micro-vibrations. This premature slip reduces the effective step length in each actuation cycle, resulting in a decrease in the average velocity of the slider. This explains why the velocity tends to decrease as frequency increases in this regime. The presence of such non-linear and chaotic behavior suggests that further model refinement is necessary to accurately capture the dynamics at high-frequency excitation.

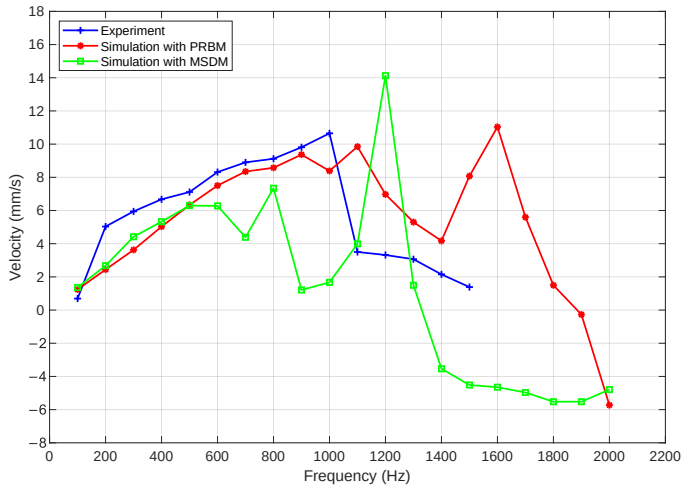


Figure 6. Comparison of slider velocity as a function of driving frequency between experimental results [18] and numerical simulations using the PRBM and MSDM at a preload of 20 N.

It should be noted that the proposed framework has been validated against published experimental results [18], ensuring its reliability without the need for additional prototype testing. Furthermore, the comparative analysis with the MSDM—commonly used in prior studies—reinforces the superior accuracy and adaptability of the proposed approach, highlighting its novelty and practical value.

The simulation results using the MSDM are also examined and compared with experimental data. As illustrated in Figure 6, this model generally follows the same overall trend as the PRBM, capturing the linear frequency–velocity relationship at low frequencies. However, its accuracy is notably lower. Specifically, the MSDM only reliably replicates the linear behavior up to approximately 500 Hz, whereas the PRBM maintains good agreement up to 900 Hz. When comparing modeling accuracy, the MSDM exhibits a significantly larger deviation from the experimental results. A quantitative evaluation of the relative modeling error in the frequency range from 100 Hz to 1000 Hz reveals that the PRBM achieves a root mean square error (RMSE) of approximately 20.19%, while the MSDM results in a substantially higher error of around 51.65%.

This highlights the limited predictive capability of the MSD approach, particularly in capturing the dynamic response of the system beyond low-frequency excitation. The primary reason for this discrepancy lies in the fundamental simplicity of the MSDM. In this approach, the entire dynamics of the compliant four-bar mechanism are approximated using a lumped mass–spring–damper system. The dynamic parameters are estimated

empirically through system identification techniques, rather than being derived from the actual structural and geometric properties of the mechanism. As a result, the model fails to capture the full range of dynamic behaviors exhibited by the real system, especially those influenced by the complex deformation characteristics of the flexure hinges. In contrast, the PRBM provides a more detailed and physically accurate representation of the mechanism. It incorporates essential design parameters of the compliant joints and better reflects the distributed flexibility and energy storage characteristics inherent in the structure. This enables the PRBM to more accurately simulate the system's dynamic behavior across a wider frequency range. This distinction underscores the key advantage of the proposed PRBM-based modeling approach over simpler lumped-parameter alternatives, such as the MSDM.

It is important to note that the improved prediction accuracy of the PRBM is not merely a consequence of parameter fitting. To ensure a fair comparison, both the PRBM and MSDM models were initialized with identical parameter sets wherever possible. Key parameters such as the friction coefficients, preload force, and piezoelectric properties were derived directly from experimental data and reused consistently across both models. Only the lumped parameters required by the MSDM (i.e., equivalent stiffness, damping, and mass terms) were fitted separately, since these cannot be mapped structurally from the prototype geometry. Therefore, the superior performance of the PRBM should be attributed to its ability to capture flexure compliance, distributed stiffness, and non-linear stick–slip transitions with higher structural fidelity, rather than to differences in parameter mapping.

It should be noted that experimental uncertainties, such as sensor resolution, signal noise, and mechanical backlash, may slightly influence the RMSE values. Nevertheless, because the RMSE calculation spans multiple frequency points and both models are compared to the same experimental dataset, such errors do not alter the conclusion that the PRBM achieves a substantially lower modeling error than the MSDM.

The three subfigures in Figure 7 present a comparison between experimental data and numerical simulations using the MSDM under variations in three key parameters: the equivalent moving mass m_e, the equivalent stiffness coefficient k_e, and the equivalent damping coefficient c_e. The reason for investigating these three cases stems from the nature of the MSD modeling approach itself. When employing the MSDM, the real system is significantly simplified into an equivalent lumped model consisting of a mass, a spring, and a damper. The associated parameters are typically derived through a combination of dynamic system identification and engineering experience. The goal is to determine a reasonably optimal set of parameters that allows the simulation to approximate experimental behavior as closely as possible. However, in order to assess the sensitivity of the simulation results to each individual parameter, we deliberately varied them by approximately one order of magnitude above and below their nominal values. This allows us to observe how strongly the velocity–frequency response depends on each parameter and evaluate the robustness of the model.

From the results, it can be observed that varying the mass, stiffness, or damping values around the nominal set does not significantly change the general behavior of the simulation. The shape and trend of the velocity–frequency response remain relatively consistent across all three cases. These curves exhibit similar peaks, valleys, and non-linear characteristics, as previously seen in the simulation results with the baseline MSDM. While slight changes in amplitude and phase are present, they are not substantial enough to suggest high sensitivity. This finding reveals a key limitation of the MSD modeling approach. Since the model reduces a structurally complex and distributed-compliance mechanism into a simple lumped-parameter system, it lacks the fidelity to accurately reflect the nuanced effects of parameter variation. As a result, even significant changes to the mass, stiffness, or damping

values yield limited variation in simulation outcomes. This reinforces the notion that while the MSDM may capture general trends, it lacks the precision and sensitivity needed for detailed dynamic analysis of compliant mechanisms.

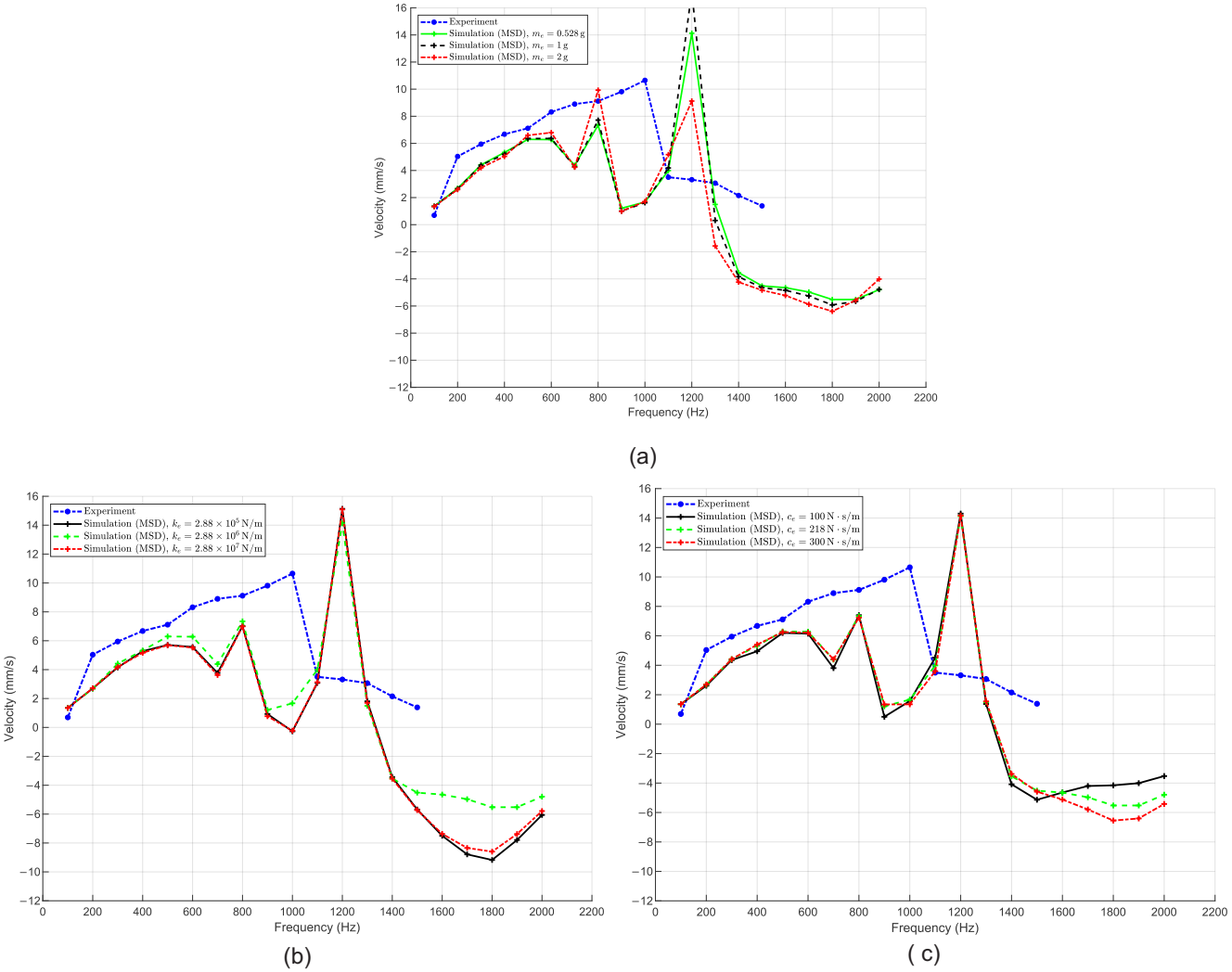


Figure 7. Comparison between experimental results and numerical simulations for different model parameters using the MSDM at a preload of 20 N: (**a**) Effect of equivalent moving mass m_e on slider velocity; (**b**) Effect of stiffness coefficient k_e on slider velocity; (**c**) Effect of damping coefficient c_e on slider velocity. Experimental data extracted from [18].

Preload is one of the key parameters that significantly affect the dynamic performance of the actuator. It plays a dual role: contributing to the generation of friction force and causing deformation in the overall system. On one hand, the friction force is essential for driving the slider; on the other hand, it helps suppress micro-vibrations. Therefore, the preload indirectly governs the velocity of the slider.

The relationship between the driving frequency and slider velocity under various preload values is shown in Figure 8. In the numerical simulations, the preload was varied from 1 N to 20 N in increments of 5 N. At a low preload of 1 N, the system exhibits non-linear behavior even at low driving frequencies, with no clear linear trend in the velocity response. When the preload increases to 5 N, linear behavior is observed up to approximately 300 Hz, beyond which non-linearity dominates. As the preload is further increased to 10 N, 15 N, and 20 N, the linear response extends to higher frequencies of around 500 Hz, 700 Hz, and 900 Hz, respectively.

These simulation results show good agreement with the experimental data, validating the influence of the preload on the system dynamics. At small preload values, the corresponding friction force is insufficient to fully suppress micro-vibrations during the stick phase, even at relatively low frequencies, leading to chaotic behavior. As the preload increases, micro-vibrations are more effectively dampened, allowing the system to maintain linear behavior over a wider frequency range. However, beyond a critical frequency threshold, chaotic behavior emerges regardless of the preload level, resulting in unstable and unpredictable changes in slider velocity.

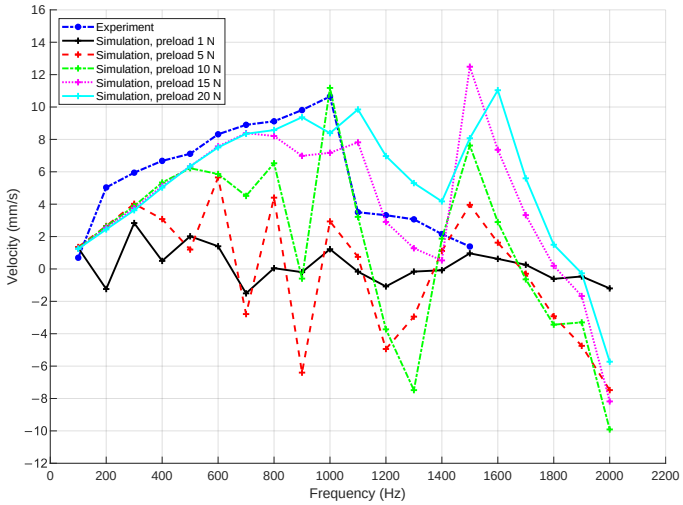


Figure 8. Simulated slider velocity responses of the actuator under various preload values using the PRBM model, compared against experimental results. As preload increases from 1 N to 20 N, the system demonstrates improved stability and extended linear response up to higher excitation frequencies.

In addition to preload, the tangential contact stiffness σ_0 and the friction coefficients μ_S (static) and μ_C (kinetic) are key parameters that influence the frictional force and, in turn, the suppression of micro-vibrations during the stick–slip process. Their impact on the actuator dynamics is illustrated in Figures 9 and 10.

Figure 9 presents the simulated slider velocity responses for different values of tangential contact stiffness, specifically, $\sigma_0 = 2 \times 10^6$ N/m, 5×10^6 N/m, and 1×10^7 N/m. The results indicate that increasing σ_0 leads to an expansion of the linear regime in the frequency–velocity relationship. Higher tangential stiffness reduces micro-vibrations during contact transitions, enabling the system to maintain regular stick–slip motion over a broader frequency range. As a result, greater actuator velocities can be achieved at higher driving frequencies. This trend confirms the critical role of contact stiffness in governing the actuator's dynamic response and optimizing its performance for high-speed applications.

Figure 10 illustrates the effect of the friction coefficients on the dynamic response of the actuator. Numerical simulations were conducted for three combinations of static and kinetic friction coefficients: $(\mu_S = 0.15, \mu_C = 0.10)$, $(\mu_S = 0.25, \mu_C = 0.15)$, and $(\mu_S = 0.3,\ \mu_C = 0.2)$. The results indicate that increasing the friction coefficients significantly enhances the system's ability to suppress micro-vibrations, leading to more stable slider motion over a broader frequency range.

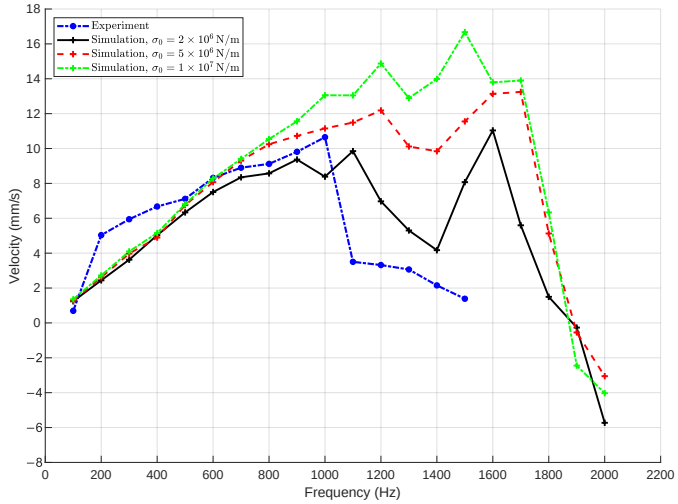


Figure 9. Comparison between experimental data and numerical simulations using the PRBM at different tangential contact stiffness values $\sigma_0 = 2 \times 10^6$, 5×10^6, and 1×10^7 N/m. Higher contact stiffness extends the linear operating range and improves velocity performance at higher frequencies.

Similar to the effect of preload, higher friction coefficients yield stronger frictional forces, which dampen chaotic oscillations during the stick–slip transitions. As a result, the actuator maintains linear velocity responses up to higher frequencies. However, beyond a certain frequency threshold, chaotic behavior emerges regardless of friction level, indicating intrinsic dynamic limits of the system. These findings reaffirm the critical role of frictional parameters in tuning the dynamic performance and stability of piezoelectric actuators.

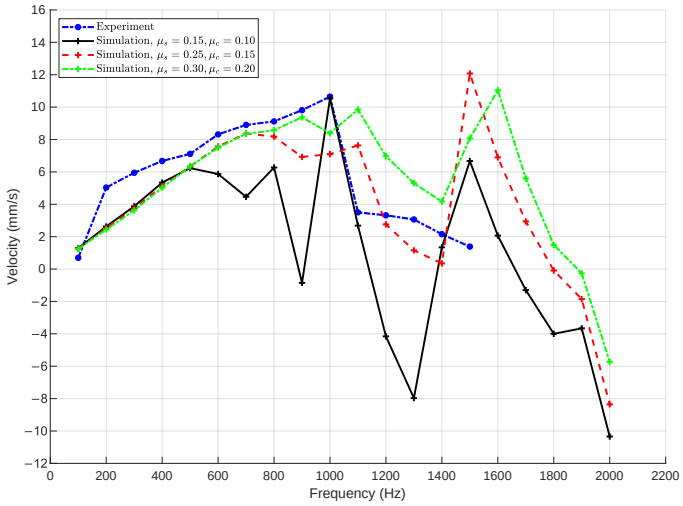


Figure 10. Influence of friction coefficients (μ_S, μ_C) on slider velocity: Higher values suppress micro-vibrations and extend stable operation to higher frequencies. PRBM simulations align well with experimental data from [18].

The influences of the design parameters of the four-bar mechanism on the dynamic behavior of the actuator are validated through the simulation results presented in Figures 11–13. These results demonstrate a significant advantage of the proposed PRBM-based modeling approach: unlike conventional MSD methods, the PRBM allows for the incorporation of the geometric and material parameters of the flexure hinge mechanism directly into the model. This capability enables a detailed assessment of how individual de-

sign parameters affect the system's dynamics, providing meaningful insights into structural optimization and performance enhancement. Such a feature aligns well with the objective of this study, which aims to establish a design-oriented dynamic model that bridges the gap between mechanical structure and system-level behavior.

Figure 11 presents the simulation results for varying the position of the center of gravity of each bar in the four-bar mechanism, characterized by the parameter β_i (with $i = 1, 2, 3$). The simulations were conducted with identical values of $\beta_i = 0°, 10°, 20°$, and $30°$ applied across all bars. The influence of this parameter on the actuator's dynamic behavior was evaluated through the frequency–velocity response curves.

The results reveal that in the low- to mid-frequency range (up to approximately 1200 Hz), the velocity curves for all cases are almost indistinguishable, indicating minimal sensitivity to the center of gravity position within this frequency range. As the driving frequency increases beyond 1200 Hz, slight deviations between the curves begin to emerge. However, these discrepancies remain small, and all simulations continue to follow a similar dynamic trend. This suggests that while the parameter β_i may influence the local inertia distribution of the links, its effect on the overall slider motion is limited for the given mechanism and operating conditions.

This result further demonstrates the capability and advantage of the proposed PRBM-based modeling approach. Since the PRBM explicitly incorporates geometric and inertial parameters—such as the mass distribution and center of gravity—it allows for detailed assessment of individual design factors on system dynamics. This is a key advantage over simplified MSDMs, which cannot account for such structural influences. Consequently, PRBM provides a more comprehensive tool for design optimization and performance evaluation of compliant mechanisms.

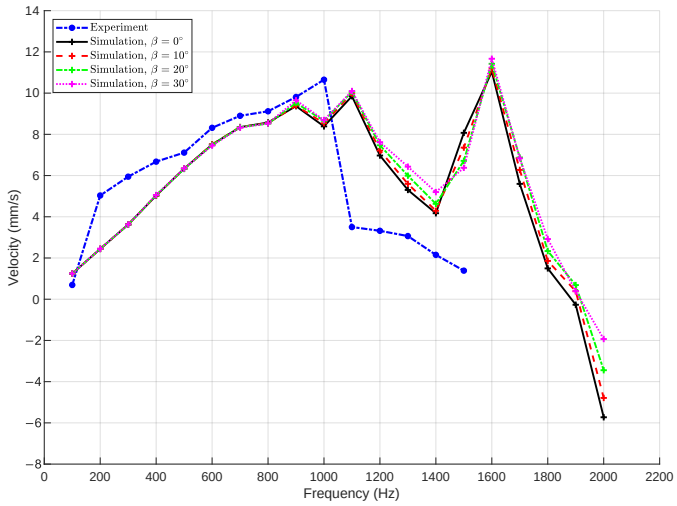


Figure 11. Frequency–velocity response under varying center-of-gravity positions, represented by angle $\beta_i = 0°, 10°, 20°, 30°$. Simulation results using the PRBM show minor influence of β_i on dynamic behavior, especially at high frequencies.

The stiffness of the flexure joint, denoted as k_u, is a critical design parameter that directly influences the dynamic response of the compliant actuator. Figure 12 presents a comparison between experimental measurements and simulation results obtained using different values of k_u, specifically 3×10^6 N/m, 3×10^7 N/m, and 8×10^7 N/m. The parameter k_u corresponds to the stiffness of the soft joint connecting the piezoelectric actuator to the four-bar mechanism.

At the lowest stiffness value, $k_u = 3 \times 10^6$ N/m, the simulation reveals highly unstable velocity responses, characterized by large oscillations and chaotic behavior even at moder-

ate excitation frequencies. Irregular motion is evident from as low as 300 Hz, indicating that insufficient joint stiffness leads to inadequate constraint of the mechanism, resulting in poor transmission of actuation forces and diminished control over system dynamics.

In contrast, simulations performed with higher stiffness values, $k_u = 3 \times 10^7$ N/m and 8×10^7 N/m, show significantly improved dynamic performance. The slider velocity remains stable and consistent across a broad frequency range up to 900 Hz, with pronounced resonance peaks observed near 1100–1300 Hz that closely match the experimental data. Among the tested values, $k_u = 3 \times 10^7$ N/m yields the best agreement with experimental results, both in terms of amplitude and resonance location. The case with $k_u = 8 \times 10^7$ N/m, while still stable, tends to overestimate velocity amplitudes and introduces secondary resonances not observed in the measurements.

These findings confirm that joint stiffness plays a decisive role in determining the actuator's dynamic characteristics. A sufficiently high k_u enhances system stability, improves the fidelity of actuation force transmission, and allows the mechanism to operate effectively under high-frequency excitation. Therefore, for reliable and predictable performance, the flexure joint must be designed with adequate stiffness that balances structural integrity with desired dynamic responsiveness.

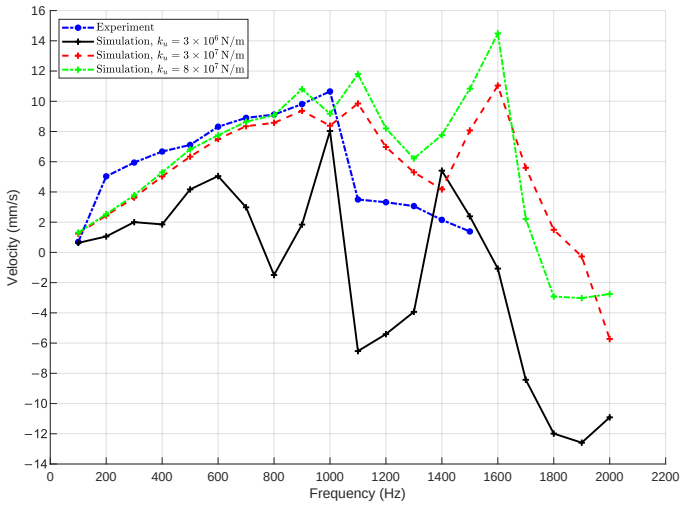


Figure 12. Simulated velocity response of the compliant actuator using the PRBM model under varying joint stiffness values $k_u = 3 \times 10^6$, 3×10^7, and 8×10^7 N/m. The simulation results are compared with experimental data to evaluate the influence of flexure joint stiffness on dynamic behavior. The case with $k_u = 3 \times 10^7$ N/m provides the best agreement with experimental results.

The influence of the position of the contact point between the slider and the contact element attached to the four-bar mechanism—denoted by the parameter l_n—is evaluated and presented in Figure 13. In the simulations, l_n is varied from 0 mm to 15 mm in increments of 5 mm. The results indicate that changes in l_n have negligible impact on the slider's velocity within the linear frequency range, particularly for excitation frequencies below 900 Hz. In this region, the velocity–frequency curves for all values of l_n closely overlap, suggesting that the position of the contact point does not significantly affect the dynamic behavior of the system. At higher frequencies beyond 900 Hz, minor discrepancies begin to emerge among the curves. These variations may be attributed to changes in the effective moment arm introduced by altering the contact point position, which could slightly affect the force transmission and energy dissipation during dynamic interaction. Nevertheless, the overall influence remains limited compared to other design parameters, such as the joint stiffness or preload. This outcome reinforces the strength of the PRBM modeling framework, which allows detailed investigation of geometric parameters like l_n.

Such analysis is not feasible with lumped-parameter models (e.g., MSD models), which abstract away structural geometry. Hence, the PRBM approach proves advantageous in evaluating the sensitivity of actuator performance to specific design features and supports design-oriented simulation analysis aligned with the objective of this study.

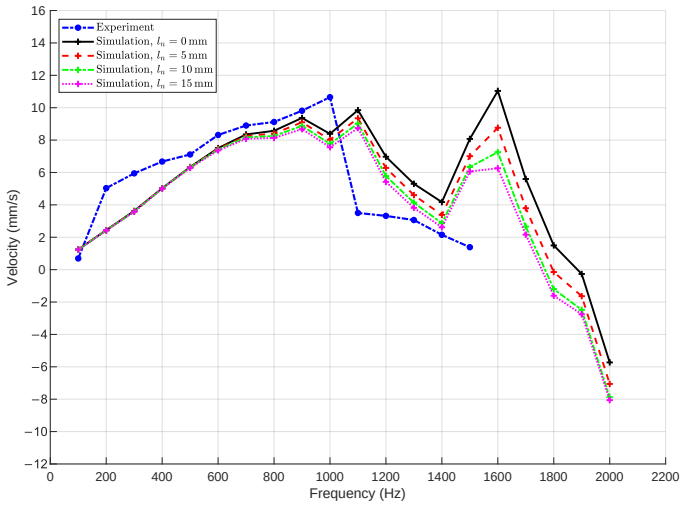


Figure 13. Dependency of slider velocity on driving frequency for different contact point positions l_n: Simulation results using the PRBM show negligible influence of l_n on system dynamics, especially below 900 Hz. Minor deviations at higher frequencies reflect small geometric effects.

The effect of slider mass m_s on the dynamic behavior of the actuator is illustrated in Figure 14. Simulations were carried out for three different masses: 0.01 kg, 0.05 kg, and 0.1 kg. The results show that a small slider mass of 0.01 kg leads to significant instability and reduced average velocity across the entire frequency range. This behavior is attributed to insufficient inertial force during the slip phase, which increases the susceptibility to backward motion and chaotic dynamics.

In contrast, with higher slider masses (0.05 kg and 0.1 kg), the system maintains more stable performance with higher velocities, particularly in the range from 600–1800 Hz. The curves for these two masses closely match the experimental data, indicating that above a certain threshold, the influence of mass becomes negligible.

These findings highlight the importance of appropriate mass selection in actuator design. While excessively small mass degrades performance, moderately higher masses improve dynamic stability without adversely affecting velocity output.

Discussion of sensitivity results

The quantitative sensitivity analysis presented in Table 5 clarifies the relative impact of key design parameters on the actuator's dynamic performance. Among all factors, the preload force F_p exerts the strongest effect, with a sensitivity of about +15% per 10% change. This finding reflects its dual role: providing sufficient normal force to sustain stick–slip motion while simultaneously suppressing micro-vibrations, thereby extending the actuator's linear operating range toward higher frequencies.

The friction pair (μ_S, μ_C) also shows a significant positive sensitivity of approximately +10%. Increasing both the static and kinetic friction coefficients enhances damping at the contact interface, which broadens the frequency range over which stable and linear velocity responses are achieved. This indicates that properly tuned friction improves system robustness without overly compromising step length.

The tangential contact stiffness σ_0 contributes a moderate effect, with an estimated sensitivity of +8%. A stiffer tangential contact reduces residual vibrations during transitions between stick and slip, enabling the system to maintain linearity and achieve higher

velocities under elevated excitation frequencies. Similarly, the flexure joint stiffness k_u demonstrates a sensitivity of about +12%. Notably, too low a stiffness induces chaotic motion and unstable transmission, while the nominal value of 3×10^7 N/m yields the closest match with experimental data, highlighting the existence of an optimal stiffness threshold.

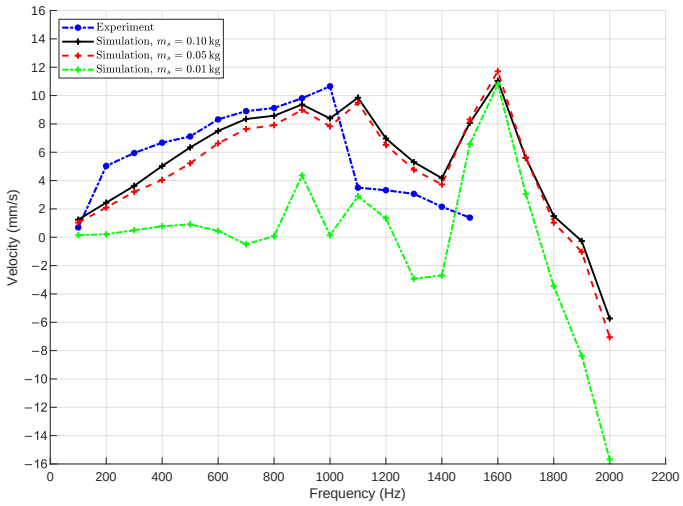


Figure 14. Dependency of the slider's velocity on driving frequency: Comparison between simulations with varying slider mass m_s and experimental data. A small mass (0.01 kg) results in unstable, low-velocity behavior due to insufficient inertia during slip, while higher masses (0.05 kg, 0.1 kg) produce stable and consistent responses.

Table 5. Quantitative sensitivity analysis of key design parameters. Sensitivity is expressed as the percentage change in the linear regime of the average velocity per 10% change in the parameter value.

Parameter (Symbol)	Nominal Value	Variation Range	Sensitivity (%$\Delta\bar{v}_{\text{lin}}$ / 10%Δp)
Preload force (F_p)	20 N	1–20 N	≈+15% (linear regime extends toward higher f as F_p increases)
Friction pair (μ_S, μ_C) [a]	(0.3, 0.2)	see Figure 10	≈+10% (higher friction broader frequency range)
Tangential contact stiffness (σ_0)	5×10^6 N/m	2×10^6–1×10^7 N/m	≈+8% (reduces micro-vibrations; higher velocity at high f)
Flexure joint stiffness (k_u)	3×10^7 N/m	3×10^6–8×10^7 N/m	≈+12% (low k_u induces chaos; ∼3×10^7 N/m best matches exp.)
Mass distribution angle (β_i)	0°	0–30°	<2% (minor influence below 1200 Hz)
Slider mass (m_s)	0.05 kg	0.01–0.10 kg	<2% (very small mass destabilizes; moderate mass improves stability)
Contact position (l_n)	5 mm	0–15 mm	<2% (negligible below 900 Hz; small deviations at high f)

Definition of linear regime. The linear regime is the maximal contiguous frequency window where the frequency–velocity relation fits a line with $R^2 > 0.98$. $\bar{v}_{\text{lin}}$ is the average velocity measured within this window after warm-up cycles. Sensitivity calculation $S_p \approx \left[(\Delta\bar{v}_{\text{lin}}/\bar{v}_{\text{lin}})/(\Delta p/p)\right] \times 100\%$, reported per 10% change in p, estimated from PRBM simulations consistent with the trends in Figures 8–14. [a] The friction *pair* (μ_S, μ_C) is varied jointly (scaled together) around the nominal (0.25, 0.15); values correspond to tested sets in Figure 10. Provenance: Nominals and ranges follow the simulations summarized in Figures 8–14; sensitivities reflect PRBM simulations benchmarked to [18].

In contrast, geometric and inertial parameters, such as the mass distribution angle β_i, slider mass m_s, and contact position l_n, have negligible impact, with sensitivities below 2–5%. Small slider masses (∼0.01 kg) may destabilize the system, but within practical ranges, variations in these parameters do not significantly shift the linear regime frequency limit.

Overall, the results establish a clear hierarchy of influence: preload force, joint stiffness, and tangential stiffness dominate actuator dynamics, while frictional parameters provide additional stabilization. Geometric factors such as β_i, m_s, and l_n exert only minor effects. These findings demonstrate the predictive capability of the PRBM–LuGre model, which not only captures overall system behavior but also quantifies parameter sensitivities, thereby guiding structural optimization and performance enhancement of flexure-hinge-based stick–slip actuators.

Performance evaluation

Table 6 compares the computational performance of three dynamic modeling approaches for compliant mechanisms: the MSDM, the Standard PRBM, and our Enhanced PRBM. The comparison is based on simulation time under different time-step resolutions, alongside their accuracy relative to experimental data.

Table 6. Comparison of computational performance and accuracy between MSDM, Standard PRBM, and Enhanced PRBM.

Modeling Approach	Accuracy (RMSE vs. Exp.)	Simulation Time	Remarks
MSDM	High error (∼51.65%)	Fastest (<1 s at $\Delta t = 10^{-7}$ s)	Simple lumped model, lacks flexure fidelity
Standard PRBM	Accurate (∼20.19%)	Slow (∼3900 s at $\Delta t = 10^{-7}$ s; fails at 10^{-8} s)	Uses Simulink/Toolbox symbolic evaluations; accurate but heavy computational overhead
Enhanced PRBM	Accurate (∼20.19%)	Fast (∼1.2 s at $\Delta t = 10^{-7}$ s; ∼11 s at 10^{-8} s)	Reformulated into closed-form expressions; same accuracy as Standard PRBM, much faster

In the Standard PRBM, the system dynamics are formulated using the Lagrangian method (Equation (1)). Kinetic and potential energies and their derivatives with respect to the generalized coordinate φ_1 are evaluated through Simulink functions and symbolic operations. While this ensures high accuracy, it incurs substantial computational overhead, especially at small time steps, where symbolic processing dominates runtime.

The Enhanced PRBM preserves the same modeling fidelity but improves computational efficiency by analytically reformulating the governing equations. Closed-form expressions are derived for the dynamic inertia coefficient $A(\varphi_1)$ (Equations (4)–(6)) and potential energy terms, removing the need for symbolic computation. This reformulation enables faster simulations while maintaining identical accuracy to the Standard PRBM.

All simulations were conducted in MATLAB 2021a on a workstation with a 12th Gen Intel(R) Core(TM) i7-12700 CPU and 64 GB of RAM. Results confirm that MSDM runs the fastest due to its simplicity but suffers from high error (≈51.65%), limiting its predictive capability. Both PRBM approaches deliver accurate results (≈20.19% RMSE vs. experiment). However, the Standard PRBM requires over 3900 s to complete a run at $\Delta t = 10^{-7}$ s and fails at $\Delta t = 10^{-8}$ s, while the Enhanced PRBM completes the same simulations in just 1.185 s and 11.067 s, respectively.

These findings demonstrate that the Enhanced PRBM combines the accuracy of a full compliant mechanism model with computational efficiency one to two orders of magnitude faster than the Standard PRBM. This makes it particularly suitable for high-resolution dynamic analyses and scenarios requiring fine time-step resolution or near real-time performance.

Comparison of modeling strategies

Table 7 compares three major modeling strategies—FEA, MSDM, and the proposed Enhanced PRBM—based on their capabilities in dynamic analysis of compliant piezoelectric actuators. Each method exhibits distinct advantages and limitations.

Table 7. Comparison of modeling capabilities between FEA, MSDM, and the proposed Enhanced PRBM based on key performance criteria in dynamic analysis of compliant systems.

Comparison Criteria	FEA	MSDM	Enhanced PRBM
Can it perform dynamic simulation?	**Yes**	**Yes**	**Yes**
Can it couple the dynamics of the whole system?	Limited (local contact, structural modes)	**Yes**	**Yes**
Can it consider structural design parameters?	**Yes**	No	**Yes**
Can it evaluate the influences of design parameters on the dynamics of the whole system?	Possible but computationally expensive	No	**Yes (efficient)**
Is it computationally efficient?	No (high cost)	**Yes**	**Yes**
Modeling accuracy	**High**	Low/Qualitative	**High**

Finite element analysis (FEA) provides the highest structural fidelity, capable of resolving detailed stress fields, local contact interactions, and modal responses. It can, in principle, perform transient dynamic simulations and parametric studies. However, these analyses are computationally expensive and become impractical when wide frequency sweeps or multi-parameter optimizations are required. Consequently, while FEA is valuable for validating structural integrity or local compliance, it is less suited for efficient system-level dynamic modeling.

In contrast, the mass–spring–damper model (MSDM) is computationally efficient and easy to implement for control design. Yet, its reliance on lumped parameters makes it structurally inconsistent. Flexure hinges are approximated by equivalent spring–damper elements, preventing the model from capturing non-linear geometric effects or assessing the direct influence of structural parameters. As a result, MSDM offers only qualitative agreement with experiments and lacks predictive capability for design optimization.

The proposed Enhanced PRBM offers a balanced alternative by combining structural fidelity with computational efficiency. Unlike MSDM, it explicitly incorporates the geometric and material properties of the flexure hinges, while avoiding the heavy computational load of FEA. Through analytical reformulation, the Enhanced PRBM retains the accuracy of the standard PRBM but runs orders of magnitude faster, enabling dynamic simulations, parametric sweeps, and sensitivity studies within practical time scales. This makes it particularly well suited as a design-oriented tool, bridging the gap between detailed structural modeling and efficient system-level prediction.

Overall, the comparison underscores that while FEA remains indispensable for local structural verification and MSDM for rapid prototyping, the Enhanced PRBM provides the most effective framework for dynamic analysis and optimization of compliant stick–slip actuators.

This section presents a comprehensive investigation into the influence of preload, contact properties, and structural design parameters on the dynamic performance of piezoelectric actuators. Through systematic simulations based on the pseudo-rigid-body model (PRBM), validated against experimental data, the study reveals the key factors that govern the stability, linearity, and transition to chaotic behavior in slider motion. The results underscore the critical role of preload and tangential contact stiffness in extending the frequency range over which the actuator can operate efficiently. Simultaneously, variations

in friction coefficients are shown to significantly affect micro-vibration suppression and enable higher velocity responses at increased driving frequencies. In contrast, changes in the mass distribution (via center of gravity position), contact point location, and even slider mass (above a minimum threshold) exhibit relatively minor influence on system behavior within the linear regime. These insights highlight the advantage of the PRBM framework in capturing the nuanced effects of structural parameters and support its application in the design-oriented optimization of compliant, friction-driven actuators.

4. Conclusions

This study developed an enhanced pseudo-rigid body model (PRBM) integrated with the LuGre friction formulation to investigate the dynamic behavior of flexure-hinge-based piezoelectric stick–slip actuators (PSSAs). Compared with the traditional mass–spring–damper model (MSDM) and finite element analysis (FEA), the proposed approach offers a balanced framework that preserves structural fidelity while maintaining computational efficiency. The enhanced PRBM reformulates the governing dynamic equations into closed-form expressions, thereby eliminating symbolic evaluations required in the standard PRBM. As a result, it achieves an up to two orders of magnitude improvement in simulation time while retaining the same accuracy as both experiments and the standard PRBM.

Quantitative comparisons demonstrated that the PRBM achieved a root mean square error of only 20.19% against experimental data, in contrast to 51.65% for the MSDM. Furthermore, the enhanced PRBM provided stable simulations at fine time steps ($\Delta t = 10^{-8}$ s), highlighting its suitability for transient analyses of non-linear stick–slip dynamics. A systematic sensitivity study further revealed the dominant influence of the preload force, flexure stiffness, friction coefficients, and tangential contact stiffness on extending the linear frequency–velocity regime, whereas the slider mass and geometric distribution played secondary roles.

Overall, the enhanced PRBM–LuGre framework bridges the methodological gap between high-fidelity but computationally demanding FEA and overly simplified MSDMs. It provides not only accurate prediction of transient responses but also efficient evaluation of design parameters, thereby supporting both theoretical analysis and practical optimization of next-generation compliant piezoelectric actuators. Future work will focus on extending the framework to incorporate control strategies and multi-axis actuation for broader applications in precision positioning and micro-robotics.

Author Contributions: X.-H.N.: conceptualization, methodology, numerical simulation, and writing—original draft preparation; D.-T.N.: validation, formal analysis, writing—review and editing, visualization, and supervision. All authors have read and agreed to the published version of the manuscript.

Funding: This research is funded by Hanoi University of Science and Technology (HUST) under project number T2022-PC-020.

Data Availability Statement: Data underlying the results presented in this paper are not publicly available at this time, but may be obtained from the authors upon reasonable request.

Acknowledgments: The authors would like to thank Hung-Anh Nguyen, Van-Hieu Hoang, and Tan-Phat Hoang for their insightful remarks and discussion.

Conflicts of Interest: The authors declare no conflicts of interest.

Abbreviations

The following abbreviations are used in this manuscript:

PSSAs	Piezoelectric Stick–Slip Actuators
FHMs	Flexure Hinge Mechanisms
PRBM	Pseudo-Rigid Body Model
MSDM	Mass–Spring–Damper Model
LuGre	Lund and Grenoble friction model

References

1. Eichhorn, V. Nanorobotic Handling and Characterization of Carbon Nanotubes Inside the Scanning Electron Microscope. Doctoral Dissertation, Carl von Ossietzky University of Oldenburg, Oldenburg, Germany, 2011; ISBN 9783868538441.
2. Nguyen, X.H. Simulation, Validation and Optimization of Stick-Slip Drives for Nanorobotic Applications. Doctoral Dissertation, The University of Oldenburg, Oldenburg, Germany, 2014.
3. Pohl, D.W. Dynamic piezoelectric translation devices. *Rev. Sci. Instrum.* **1986**, *58*, 54–57. [CrossRef]
4. Zhang, Z.M.; An, Q.; Li, J.W.; Zhang, W.J. Piezoelectric frictional inertia actuator: A critical review and future perspective. *Int. J. Adv. Manuf. Technol.* **2012**, *62*, 669–685. [CrossRef]
5. Hunstig, M. Piezoelectric Inertia Motors—A Critical Review of History, Concepts, Design, Applications, and Perspectives. *Actuators* **2017**, *6*, 7. [CrossRef]
6. Zhang, Z.; Fan, P.; Dong, Y.; Yu, S.; Liu, K.; Lu, X. A review of modeling and control of piezoelectric stick-slip actuators. In *Piezoelectric Actuators*; Cheng, T., Li, J., Eds.; IntechOpen: London, UK, 2022. [CrossRef]
7. Qiao, G.; Li, H.; Lu, X.; Wen, J.; Cheng, T. Piezoelectric stick-slip actuators with flexure hinge mechanisms: A review. *J. Intell. Mater. Sys. Struct.* **2022**, *33*, 1879–1901. [CrossRef]
8. Lin, Y.; An, D.; Lin, Z.; Chen, X.; Huang, W. Progress in high-performance stick-slip piezoelectric actuators: A review. *Inter. J. Smart Nano Mater.* **2024**, *15*, 652–696. [CrossRef]
9. Zhong, B.; Liao, Z.; Hu, H.; Liu, S.; He, C.; Sun, L. A Review of Recent Studies on Piezoelectric Stick-slip Actuators. *Precis. Eng.* **2025**, *94*, 175–190. [CrossRef]
10. Li, Z.; Su, Z.; Zhao, L.; Han, H.; Guo, Z.; Zhao, Y.; Sun, H. Design and Locomotion Study of Stick-Slip Piezoelectric Actuator Using Two-Stage Flexible Hinge Structure. *Micromachines* **2021**, *12*, 154. [CrossRef] [PubMed]
11. Ding, Z.; Dong, J.; Zhou, X.; Xu, Z.; Qiu, W.; Shen, C. Achieving smooth motion of stick–slip piezoelectric actuator by means of alternate stepping. *Mech. Syst. Signal Process.* **2022**, *181*, 109494. [CrossRef]
12. Huang, H.; Liu, Y.; Xu, Z.; Li, X.; Wang, K. Achieving high consistency in forward and reverse motions of stick-slip piezoelectric actuator by a symmetrical structure and optimized installation method. *Microsyst. Technol.* **2023**, *29*, 1343–1355. [CrossRef]
13. Wang, L.; Wang, H.; Wang, S.; Cheng, T. Development and evaluation of a new piezoelectric stick-slip actuator using stair type flexure hinge. *J. Intell. Mater. Syst. Struct.* **2023**, *34*, 664–671. [CrossRef]
14. Wang, L.; Zhang, Y. Design and evaluation of a bionic piezoelectric stick-slip actuator inspired by human body. *Sens. Actuators A Phys.* **2024**, *376*, 115670. [CrossRef]
15. Yang, S.; Dong, H.; Zhang, Z.; Wang, Y.; Niu, X.; Lu, X. An enhancing flexibility piezoelectric stick-slip actuator by introducing perforation of flexible hinge. *Sens. Actuators A Phys.* **2024**, *379*, 115871. [CrossRef]
16. Ye, T.; Feng, Z.; Li, Y. Design and Optimization of a Piezoelectric Stick-Slip Actuator with Distributed Compliance. *Machines* **2025**, *13*, 460. [CrossRef]
17. Zhang, T.; Ma, R.; Wang, Y.; Bian, D.; Qin, Y.; Zhang, J.; Wang, Y. A stick–slip piezoelectric actuator utilizing a special parallelogram flexible mechanism. *Rev. Sci. Instrum.* **2025**, *96*, 075001. [CrossRef]
18. Sun, P.; Lei, C.; Ge, C.; Guo, Y.; Zhu, X. A Compact Piezo-Inertia Actuator Utilizing the Double-Rocker Flexure Hinge Mechanism. *Micromachines* **2023**, *14*, 1117. [CrossRef] [PubMed]
19. Yuan, L.; Li, Y.; Wang, L.; Liu, C.; Si, X.; Zhao, Z. A piezoelectric inertial actuator operating with elliptical drive and stick-slip drive modes. *Sens. Actuators A Phys.* **2024**, *373*, 115428. [CrossRef]
20. Wang, X.; Zhu, L.; Huang, H. A dynamic model of stick-slip piezoelectric actuators considering the deformation of overall system. *J. IEEE Trans. Indus. Elect.* **2020**, *68*, 11266–11275. [CrossRef]
21. Shao, Y.; Xu, M.; Shao, S.; Song, S. Effective dynamical model for piezoelectric stick–slip actuators in bi-directional motion. *Mech. Syst. Signal Process.* **2020**, *145*, 106964. [CrossRef]
22. Wang, J.; Huang, H.; Wang, Z.; Qin, F.; Zhao, H. Development and analysis of a dynamic model for parasitic motion principle piezoelectric actuator. *Mech. Syst. Signal Process.* **2021**, *147*, 107079. [CrossRef]
23. Ling, M.; Zhang, X. Coupled dynamic modeling of piezo-actuated compliant mechanisms subjected to external loads. *Mech. Mach. Theory* **2021**, *160*, 104283. [CrossRef]
24. Yang, S.; Li, Y.; Qiao, G.; Zhang, X.; Lu, X. Topology Optimization Methods for Flexure Hinge Type Piezoelectric Actuators. In *Piezoelectric Actuators*; IntechOpen: London, UK, 2022.

25. Wang, J.; Huang, H.; Zhao, H. Model-based optimization for structure dimension and driving signal of a stick-slip piezoelectric actuator. *Mech. Syst. Signal Process.* **2022**, *164*, 108191. [CrossRef]
26. Ling, M.; Howell, L.L.; Cao, J.; Chen, G. Kinetostatic and dynamic modeling of flexure-based compliant mechanisms: A survey. *Appl. Mech. Rev.* **2020**, *72*, 030802. [CrossRef]
27. Dahl, P.R. *A Solid Friction Model*; Aerospace Corp.: El Segundo, CA, USA, 1968.
28. de Wit, C.C.; Olsson, H.; Astrom, K.J.; Lischinsky, P. A new model for control of systems with friction. *IEEE Trans. Autom. Control* **1995**, *40*, 419–425. [CrossRef]
29. Dupont, P.; Hayward, V.; Armstrong, B. Altpeter, F. Single state elastoplastic friction models. *IEEE Trans. Autom. Control* **2002**, *47*, 787–792. [CrossRef]
30. Merry, R.J.; Maassen, M.G.; van de Molengraft M.J.; Van de Wouw, N.; Steinbuch, M. Modeling and waveform optimization of a nano-motion piezo stage. *IEEE/ASME Trans. Mechatron.* **2010** *16*, 615–626. [CrossRef]
31. Hunstig, M.; Hemsel, T.; Sextro, W. Modelling the friction contact in an inertia motor. *J. Intell. Mater. Sys. Struct.* **2013**, *24*, 1380–1391. [CrossRef]
32. Teidelt, E.; Willert, E.; Filippov, A.E.; Popov, V.L. Modeling of the dynamic contact in stick-slip microdrives using the method of reduction of dimensionality. *J. Phys. Mesomech.* **2012**, *15*, 287–292. [CrossRef]
33. Nguyen, H.X.; Teidelt, E.; Popov, V.L.; Fatikow, S. Modeling and waveform optimization of stick-slip microdrives using the method of dimensionality reduction. *Arch. Appl. Mech.* **2016**, *86*, 1771–1785. [CrossRef]
34. Nguyen, X.-H.; Mau, T.-H.; Meyer, I.; Dang, B.-L.; Pham, H.-P. Improvements of Piezo-Actuated Stick–Slip Micro-Drives: Modeling and Driving Waveform. *Coatings* **2018**, *8*, 62. [CrossRef]
35. Breguet, J.M. Stick and Slip Actuators. Doctoral Dissertation, Ecole Polytechnique Federale De Lausanne (EPFL), Lausanne, Switzerland, 1998.
36. Bergander, A.; Breguet, J.M. Performance improvements for stick-slip positioners. In Proceedings of the 2003 International Symposium on Micromechatronics and Human Science, Nagoya, Japan, 19–22 October 2003. [CrossRef]
37. Peng, J.Y.; Chen, X.B. Modeling of Piezoelectric-Driven Stick-Slip Actuators. *IEEE/ASME Trans. Mechatron.* **2011**, *16*, 394–399. [CrossRef]
38. Edeler, C.; Meyer, I.; Fatikow, S. Modeling of stick-slip micro-drives. *J. Micro-Nano Mechatron.* **2011**, *6*, 65–87. [CrossRef]
39. Zhang, W.J.; Li, Q.; Guo, L. S. Integrated design of mechanical structure and control algorithm for a programmable four-bar linkage. *IEEE/ASME Trans. Mech.* **1999**, *4*, 354–362. [CrossRef]
40. Merken, P. La Fonction Guidage en microméCanique. Master's Thesis, University of Liège, Liège, Belgium, 2006.

Disclaimer/Publisher's Note: The statements, opinions and data contained in all publications are solely those of the individual author(s) and contributor(s) and not of MDPI and/or the editor(s). MDPI and/or the editor(s) disclaim responsibility for any injury to people or property resulting from any ideas, methods, instructions or products referred to in the content.